RSC Advances

PAPER

View Article Online
View Journal | View Issue

Check for updates

Cite this: *RSC Adv.*, 2024, **14**, 33459

Thermal investigation of $NbSe_2$ nanoparticles synthesized through a temperature-dependent sonochemical method

Shivani R. Bharucha,[a] Mehul S. Dave,*[a] Sunil H. Chaki[b] and Tushar A. Limbani *[cd]

Due to their unique size-dependent properties, transition metal di-chalcogenide nanoparticles are trending in research for their potential to revolutionize next-generation electronics, energy storage, and catalytic processes. This study addresses the effect of temperature when synthesizing $NbSe_2$ nanoparticles *via* the sonochemical method at three different temperatures, room temperature (R.T.), 70 °C, and 100 °C. Energy Dispersive X-ray Analysis (EDAX) confirmed the high purity of $NbSe_2$, with the sample synthesized at 70 °C, displaying the accurate stoichiometric ratio. X-ray diffraction (XRD) analysis revealed that all samples maintained the hexagonal phase of $NbSe_2$, with 70 °C exhibiting superior crystallinity due to their crystallite size, lowest dislocation density, and minimal internal strain. Thermogravimetric analysis (TGA) and differential thermogravimetric (DTG) analyses, demonstrated that the sample synthesized at 70 °C had the highest thermal stability, with the lowest total weight loss and most consistent mass loss behavior. Kinetic parameters were evaluated using the Kissinger–Akahira–Sunose (KAS) and Flynn–Wall–Ozawa (FWO) methods, determining activation energy (E_a), pre-exponential factor (A), change in activation enthalpy (ΔH^*), change in activation entropy (ΔS^*), and Gibbs free energy change (ΔG^*). Also, the sample synthesized at 70 °C exhibited the highest E_a, indicating superior thermal stability and favorable reaction kinetics. The findings underscore the significant impact of synthesis temperature on the structural and thermal properties of $NbSe_2$ nanoparticles, with the sample synthesized at 70 °C demonstrating optimal characteristics. This study provides valuable insights into temperature-dependent synthesis and the thermal behavior of $NbSe_2$ nanoparticles, highlighting their potential in various technological applications.

Received 15th July 2024
Accepted 16th October 2024

DOI: 10.1039/d4ra05108d

rsc.li/rsc-advances

Open Access Article. Published on 22 October 2024. Downloaded on 1/27/2026 10:50:57 AM.
This article is licensed under a Creative Commons Attribution-NonCommercial 3.0 Unported Licence.

1. Introduction

Transition metal dichalcogenides (TMDs) have garnered significant attention in recent years due to their unique properties and potential applications in various fields, including electronics, catalysis, and energy storage.[1–5] Niobium diselenide ($NbSe_2$) stands out for its distinctive layered structure and intriguing electronic, optical, and thermal characteristics.[6,7] $NbSe_2$ nanoparticle (NPs) synthesis presents an opportunity to further explore and exploit these properties, particularly in nanoscale applications where size, morphology, and thermal stability are crucial.[8–10]

However, a thorough understanding of how synthesis conditions, particularly the temperature, affect these properties is still largely unknown.[11–17] Advanced thermal analysis approaches are needed for the thorough investigation of the thermal stability and phase transitions of $NbSe_2$ NPs, which are crucial for their successful implementation in sensors, photodetectors, and thermoelectric devices.[18,19]

This research closes the information gap regarding the impact of synthesis temperature on the structural and thermal characteristics of $NbSe_2$ NPs. By providing a controlled environment for adjusting synthesis parameters, the sonochemical synthesis approach makes it possible to investigate the connection between synthesis conditions and NPs characteristics systematically.[20,21] Through structural characterization and thermal analysis methods, including thermogravimetric (TG), and derivative thermogravimetry (DTG), this work seeks to elucidate the links between the synthesis, structure, and properties of $NbSe_2$ NPs.[22] These discoveries will contribute to the advancement of nanomaterials and increase the range of practical uses for $NbSe_2$ NPs through the improvement of their performance in numerous technological applications and streamlining the fabrication process. Although extensive

[a]*N. V. Patel College of Pure & Applied Science, Charutar Vidya Mandal University, Gujarat 388120, India. E-mail: mehul@nvpas.edu.in*

[b]*Department of Physics, Sardar Patel University, Gujarat 388120, India*

[c]*C. L. Patel Institute of Studies and Research in Renewable Energy, Charutar Vidya Mandal University, New Vallabh Vidyanagar, Gujarat 388121, India. E-mail: tusharlimbani97@gmail.com*

[d]*Solar Energy Department, School of Energy Technology, Pandit Deendayal Energy University, Gandhinagar, Gujarat 382007, India*

© 2024 The Author(s). Published by the Royal Society of Chemistry

Open Access Article. Published on 22 October 2024. Downloaded on 1/27/2026 10:50:57 AM. This article is licensed under a Creative Commons Attribution-NonCommercial 3.0 Unported Licence.

research has been conducted on bulk $NbSe_2$,[6,7,16,19,23,24] there has been comparatively less focus on $NbSe_2$ NPs using thermal analysis techniques.

The synthesis of NPs using the sonochemical method[25–28] offers several advantages, including uniform particle size distribution, high purity, and controlled crystallinity. This method employs ultrasonic waves to facilitate the nucleation and growth of NPs, enabling the precise manipulation of synthesis conditions to tailor the properties of the resulting materials.[29] In our previous report, the authors successfully synthesized $NbSe_2$ nanoparticles at room temperature.[22] To investigate the reproducibility and study on effect of synthesis temperature, the authors again synthesized $NbSe_2$ at room temperature (R.T.), 70 °C, and 100 °C, observing significant variations in the compositional, structural, and thermal properties of the NPs.

To understand the elemental composition and purity of the synthesized NPs, the energy dispersive X-ray analysis (EDAX) is performed. The X-ray diffraction (XRD) techniques were used to determine, whether the samples maintained the hexagonal phase of $NbSe_2$, and favorable structural properties, with the largest crystallite size, lowest dislocation density, internal strain, and better crystallinity.[20] Thermal analysis, including TG and DTG analysis, was conducted to evaluate the thermal stability and decomposition behavior of the synthesized NPs.[30,31] The authors employed model-free methods, specifically the Kissinger–Akahira–Sunose (KAS) and Flynn–Wall–Ozawa (FWO) methods further to understand the kinetic parameters of the thermal decomposition process. These methods allowed authors to determine the activation energy (E_a), pre-exponential factor (A), change in activation enthalpy (ΔH^*), change in activation entropy (ΔS^*), and Gibbs free energy change (ΔG^*) for the synthesized samples.[32,33]

This study comprehensively investigates the thermal behavior of $NbSe_2$ NPs synthesized *via* the temperature-dependent sonochemical method synthesis. The findings highlight the critical role of synthesis temperature in determining the compositional, structural, and thermal properties of $NbSe_2$ NPs. These results underscore the potential of optimizing synthesis conditions to tailor the properties of $NbSe_2$ NPs for various advanced applications.

2. Results and discussion

2.1. Energy dispersive X-ray analysis (EDAX)

The EDAX results of $NbSe_2$ NPs synthesized at R.T., 70 °C, and 100 °C using the sonochemical method revealed crucial insights into their elemental composition and purity. The observed and standard atomic percentages of Nb and Se are shown in Fig. 1, based on an average of five observations at different areas of the sample surfaces shown in Fig. 2. In Fig. 1 for all three samples, the spectra display prominent peaks corresponding to niobium (Nb) and selenium (Se), confirming the presence of these elements in the synthesized nanoparticles. The Nb and Se peaks were observed around 2–2.5 keV at the 100 °C sample. These peaks indicate a higher degree of Nb–Se interaction or alloying at this temperature, which is less pronounced in the R.T. and 70 °C samples due to differences in the synthesis conditions.

The EDAX spectra for $NbSe_2$ nanoparticles reveal a clear temperature-dependent variation in peak intensity. At R.T. and 70 °C, the primary peaks are lower, while at 100 °C, the primary peak is significantly higher. This can be attributed to increased crystallinity and improved particle morphology at higher

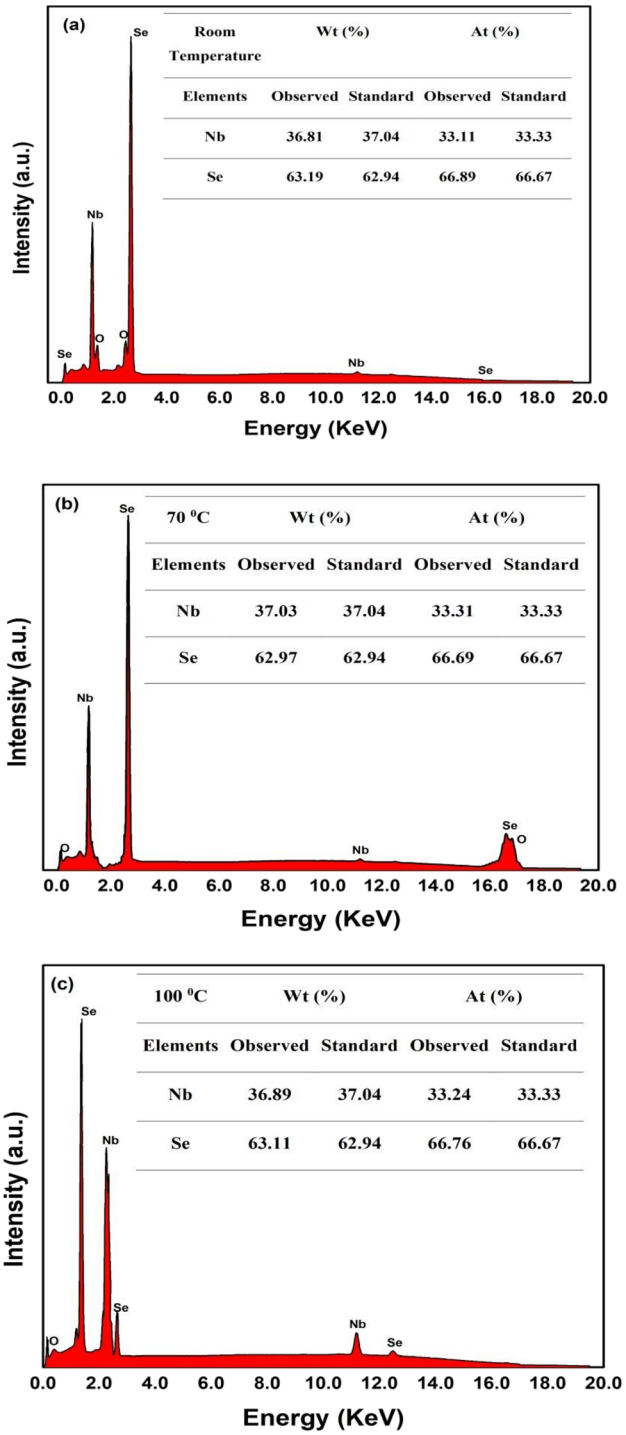

Fig. 1 The EDAX spectrum of $NbSe_2$ NPs synthesized at (a) R.T., (b) 70 °C, and (c) 100 °C.

© 2024 The Author(s). Published by the Royal Society of Chemistry

Open Access Article. Published on 22 October 2024. Downloaded on 1/27/2026 10:50:57 AM.
This article is licensed under a Creative Commons Attribution-NonCommercial 3.0 Unported Licence.

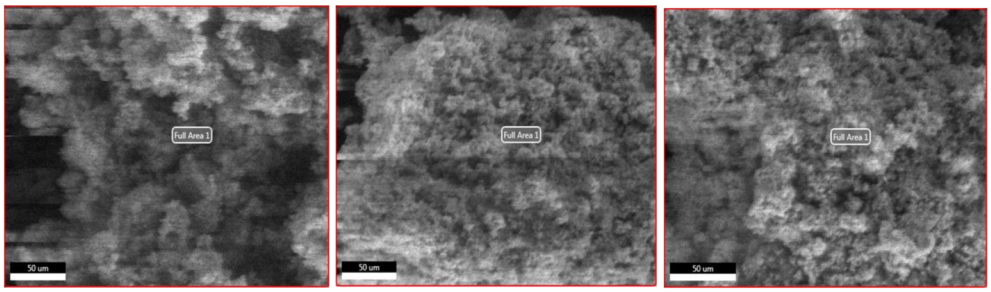

Fig. 2 Shows the microscopic image from EDAX for $NbSe_2$ nanoparticles synthesized at (a) R.T., (b) 70 °C, (c) 100 °C respectively.

synthesis temperatures. The enhanced atomic mobility at 100 °C promotes better crystallite growth, resulting in denser, more uniform particles that produce stronger X-ray interactions, reflected in the more intense EDAX peaks. In contrast, lower temperatures lead to less organized and potentially smaller crystallites, explaining the reduced peak intensities.

The observed weight percentages of Nb in samples R.T., 70 °C, and 100 °C are 36.81%, 37.03%, and 36.89%, respectively, close to the standard value of 37.04%. Similarly, the observed weight percentages of Se are 63.19%, 62.97%, and 63.11%, respectively, aligning closely with the standard value of 62.94%. The atomic percentages of Nb and Se also consistently match the standard values across all samples, with Nb around 33.11% to 33.24% and Se around 66.76% to 66.89%.

The microscopic images in Fig. 2 present the surface images of $NbSe_2$ nanoparticles synthesized at three different temperatures: R.T., 70 °C, and 100 °C. These images are associated with the regions where EDAX data were collected to analyze the nanoparticles' elemental composition.

However, these findings suggest that increasing the synthesis temperature may lead to changes in the stoichiometric composition of the synthesized NPs. Also, the synthesis temperature significantly impacts the elemental composition of the synthesized $NbSe_2$ NPs.

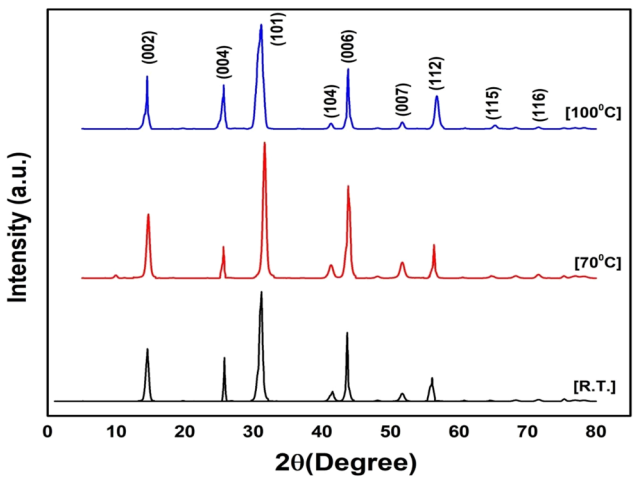

Fig. 3 The XRD patterns of $NbSe_2$ NPs samples synthesized at R.T., 70 °C, and 100 °C.

2.2. X-ray diffraction (XRD)

The XRD analysis of synthesized $NbSe_2$ NPs provided valuable information regarding their crystal structure and phase purity. The XRD patterns exhibited distinct diffraction peaks corresponding to the (101) planes of hexagonal $NbSe_2$, shown in Fig. 3. From the image revealed that the synthesis method employed in this study does not result in alterations to the structure and phase of $NbSe_2$, even with varying temperatures. This is supported by the XRD data, well matched with standard JCPDS no. 018-0923 (ref. 34 and 35) which primarily show similar peak positions and patterns across all samples. The presence of very small intensities and unlabelled peaks in the XRD pattern might originate from instrumental noise. The other structural parameters such as crystallite size, dislocation density, and main internal strain of all the samples are tabulated in Table 1.

Based on the data obtained for the synthesized samples, the data presented in Table 1 is justified based on detailed experimental observations and analysis. The well-matched observed lattice constants with the standard for all samples are consistent at 3.44 Å for $a = b$ and 12.56 Å for c, which confirms that the crystal structure remains stable across different synthesis temperatures. The crystallite size increases slightly with temperature, reaching 15.71 nm at 100 °C, signifying that higher temperatures promote larger crystal growth. The dislocation density decreases from 5.40×10^{-3} at R.T. to 4.74×10^{-3} at 70 °C and then returns to 5.40×10^{-3} at 100 °C, indicating fewer defects at 70 °C and a trend towards higher defect density at 100 °C. The main internal strain decreases from 0.57 at R.T. to 0.43 at 70 °C, and then increases again to 0.57 at 100 °C, reflecting the effect of temperature on internal stress. These observations are consistent with the known impact of synthesis temperature on crystallite growth, defect density, and internal strain, providing a comprehensive justification for the data presented in the table.

Table 1 The structural parameters of $NbSe_2$ NPs samples synthesized at R.T., 70 °C, and 100 °C

Sample	Crystallite size (D) (nm)	Dislocation density (δ) $\times 10^{-3}$	Main internal strain (ε)
R.T.	14.94	5.40	0.57
70 °C	15.12	4.74	0.43
100 °C	15.71	5.40	0.57

Open Access Article. Published on 22 October 2024. Downloaded on 1/27/2026 10:50:57 AM.
This article is licensed under a Creative Commons Attribution-NonCommercial 3.0 Unported Licence.

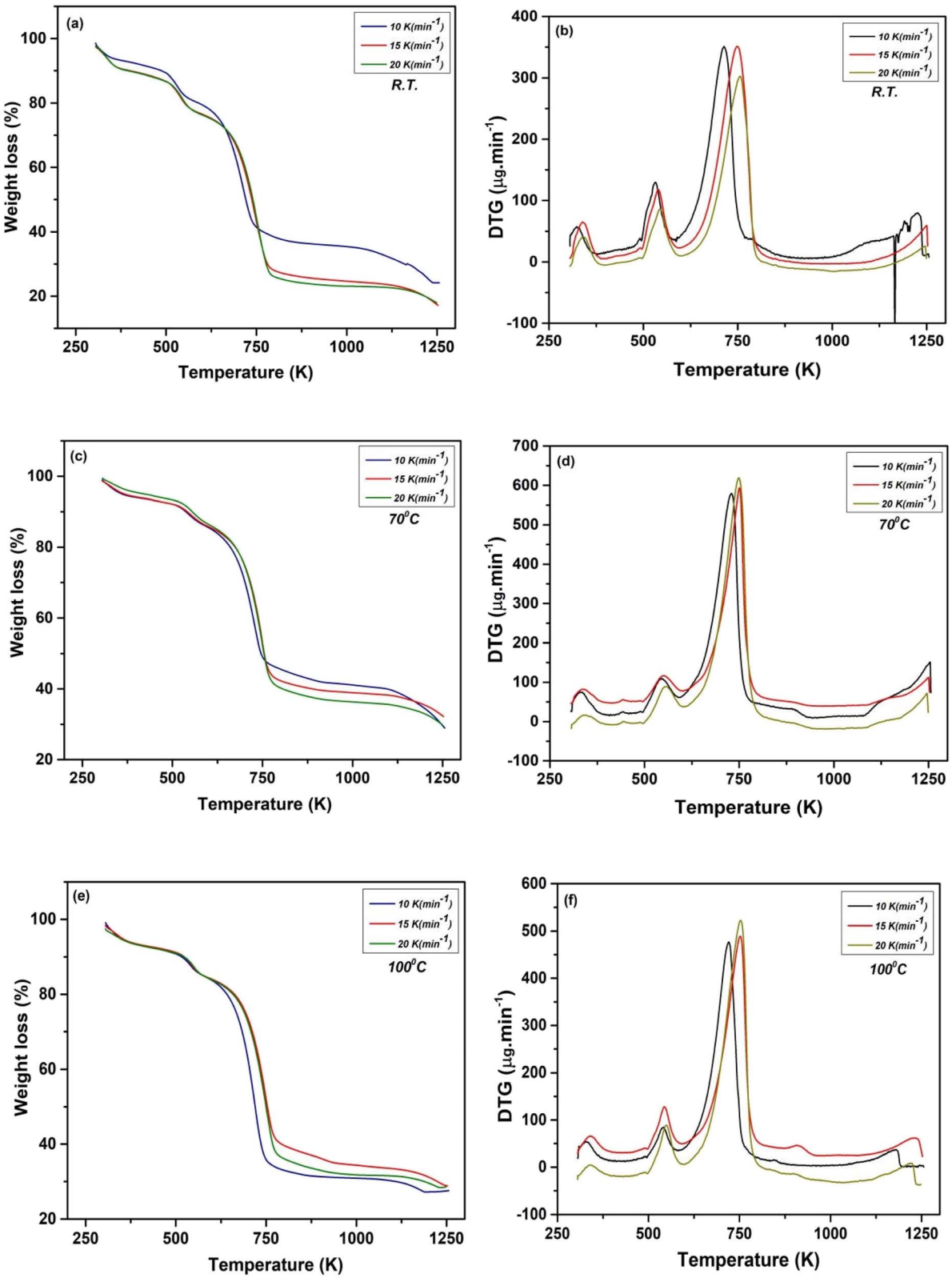

Fig. 4 TG curves of $NbSe_2$ NPs synthesized at (a) R.T., (c) 70 °C, (e) 100 °C and DTG curve of $NbSe_2$ NPs synthesized at (b) R.T., (d) 70 °C and (f) 100 °C.

2.3. Thermal analysis

2.3.1. Thermal gravimetric (TG) analysis. TG technique was used to study the mass of material changes exposed under temperatures. The key aspect of TG control was the increase in temperature. The recorded TG curves for all the samples are shown in Fig. 4(a), (c) and (e). All samples show continuous

© 2024 The Author(s). Published by the Royal Society of Chemistry

Open Access Article. Published on 22 October 2024. Downloaded on 1/27/2026 10:50:57 AM. This article is licensed under a Creative Commons Attribution-NonCommercial 3.0 Unported Licence.

Table 2 The temperature range and obtained weight loss (%) for $NbSe_2$ NPs synthesized at R.T., 70 °C, and 100 °C

		Mass loss (%)				
		Temperature range (K)				Total weight loss (%)
Sample	Heating rate	305–498	499–604	605–1203	1204–1260	305–1260
R.T.	10	10.16	9.87	49.75	4.65	74.43
	15	9.63	9.43	50.00	3.31	72.37
	20	9.89	9.56	49.94	2.42	71.81
70 °C	10	6.77	6.90	51.07	5.33	70.07
	15	6.13	7.13	53.42	2.91	69.59
	20	6.56	6.55	50.33	3.13	66.57
100 °C	10	8.25	7.37	56.29	0.34	72.25
	15	7.15	7.37	52.86	2.18	69.56
	20	6.50	7.34	54.24	0.92	69.00

weight loss in all heating rates and observe that the decomposition occurs in four steps and is substantiated by the presence of four peaks in corresponding DTG curves (Fig. 4(b), (d) and (f)). The temperature ranges for weight loss calculation in TGA were determined based on the peak temperature ranges observed in the DTG curve. The magnitude of weight loss in four steps for samples R.T., 70 °C, and 100 °C are tabulated in Table 2. The concurrently recorded DTG curves for samples R.T., 70 °C, and 100 °C, as depicted in Fig. 4(b), (d) and (f), exhibit four distinct peaks across all three heating rates, indicating a four-step decomposition process with corresponding weight losses.

Based on the data obtained from the thermal analysis, revealed that the sample at 70 °C shows higher thermal stability and consistent mass loss behavior compared to R.T., and 100 °

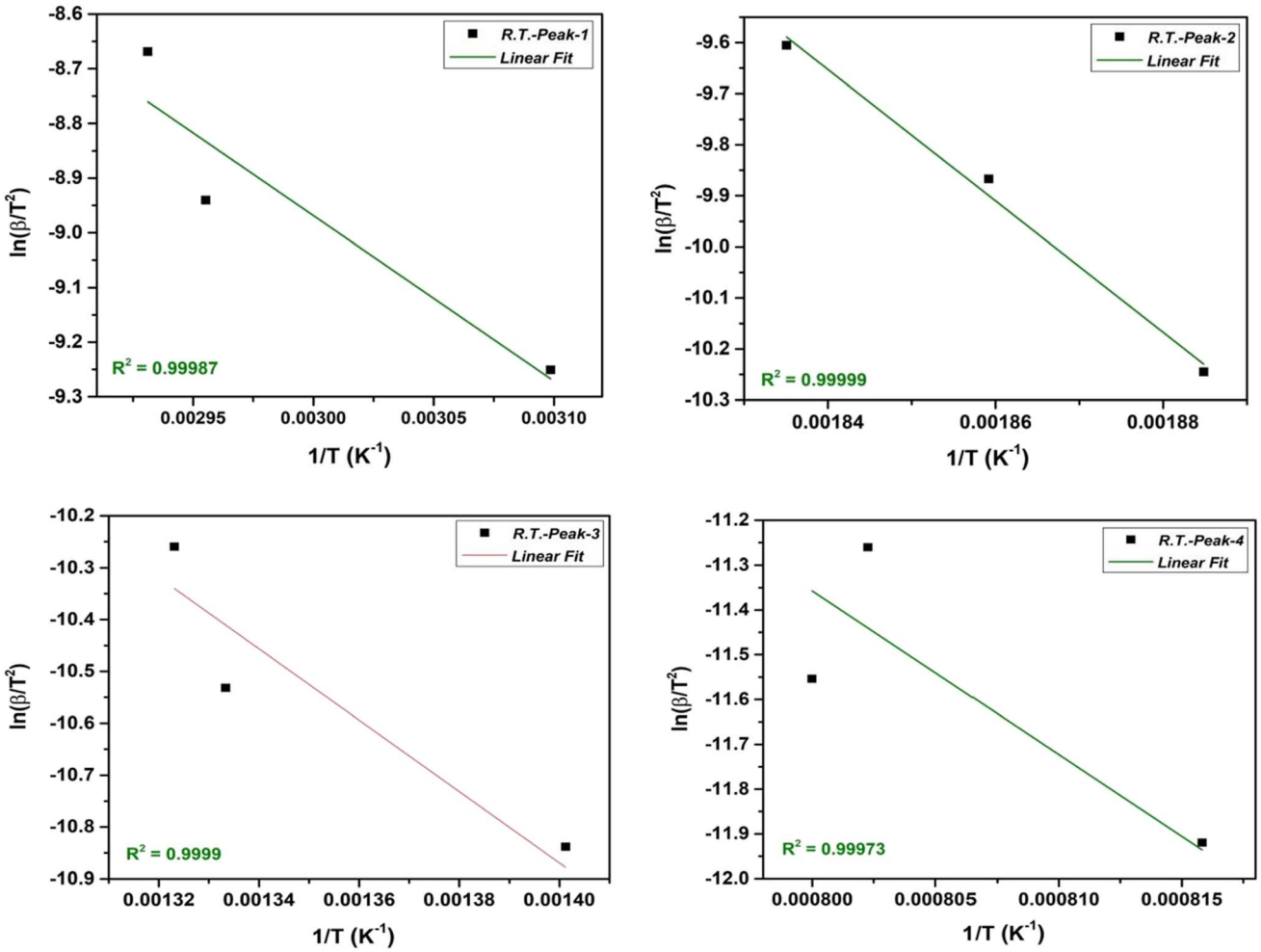

Fig. 5 The KAS plot of four-step decomposition for $NbSe_2$ NPs sample synthesized at R.T.

Open Access Article. Published on 22 October 2024. Downloaded on 1/27/2026 10:50:57 AM. This article is licensed under a Creative Commons Attribution-NonCommercial 3.0 Unported Licence.

C. The total weight loss across the temperature range of 305–1260 K at 70 °C is the lowest, ranging from 70.07% to 66.57% indicating less decomposition and better thermal stability. This may be due to a more stable intermediate phase formed at this temperature, leading to reduced decomposition during thermal analysis. In contrast, R.T., and 100 °C showed higher total weight losses, up to 74.43% and 72.25%, respectively. The heating rate also affected mass loss, with higher rates slightly reducing total weight loss, but the trend remained that at 70 °C consistently lost the least total weight.[36,37]

2.3.2. Kinetic parameters. There are two different mathematical schemes to evaluate kinetic parameters for the thermal decomposition of $NbSe_2$ NPs. The first model-based methods depend on the different reaction models. The second approach is the model-free method also called the iso-conversional technique. Here the authors consider model-free methods for evaluating kinetic parameters of synthesized $NbSe_2$ NPs at R.T., 70 °C, and 100 °C. Here the two iso-conventional methods considered for obtained kinetic parameters are KAS and FWO.

2.3.2.1. Kissinger–Akahira–Sunose (KAS) method. The KAS method is a widely used approach for determining kinetic parameters, specifically the E_a and A from thermal analysis data. The integral KAS method originates from the Coats–Redfern (CR) estimation.[22,38,39] The method is based on the eqn (1) as follows;[40]

$$\ln\left(\frac{\beta}{T^2}\right) = \ln\left(\frac{AR}{E_a f(\alpha)}\right) - \frac{E_a}{RT} \quad (1)$$

E_a is the activation energy, β is the heating rate, T is the absolute temperature of corresponding DTG peaks, A is the phonon frequency factor, R is the universal gas constant, and $f(\alpha)$ is the integral transformation function.

The KAS method involves taking advantage of the Arrhenius equation by plotting the natural logarithm of the heating rate $\ln\left(\frac{\beta}{T^2}\right)$ *vs.* $1/T$ at various conversion levels during thermal analysis experiments. The KAS plot of the four-step decomposition peaks for $NbSe_2$ NPs at R.T., 70 °C, and 100 °C is shown in Fig. 5, 6, and 7 respectively.

The slope and intercept allow evaluation of the kinetic parameters such as activation energy and phonon frequency factor (A),

$$E_a = -(\text{slope} \times R) \quad (2)$$

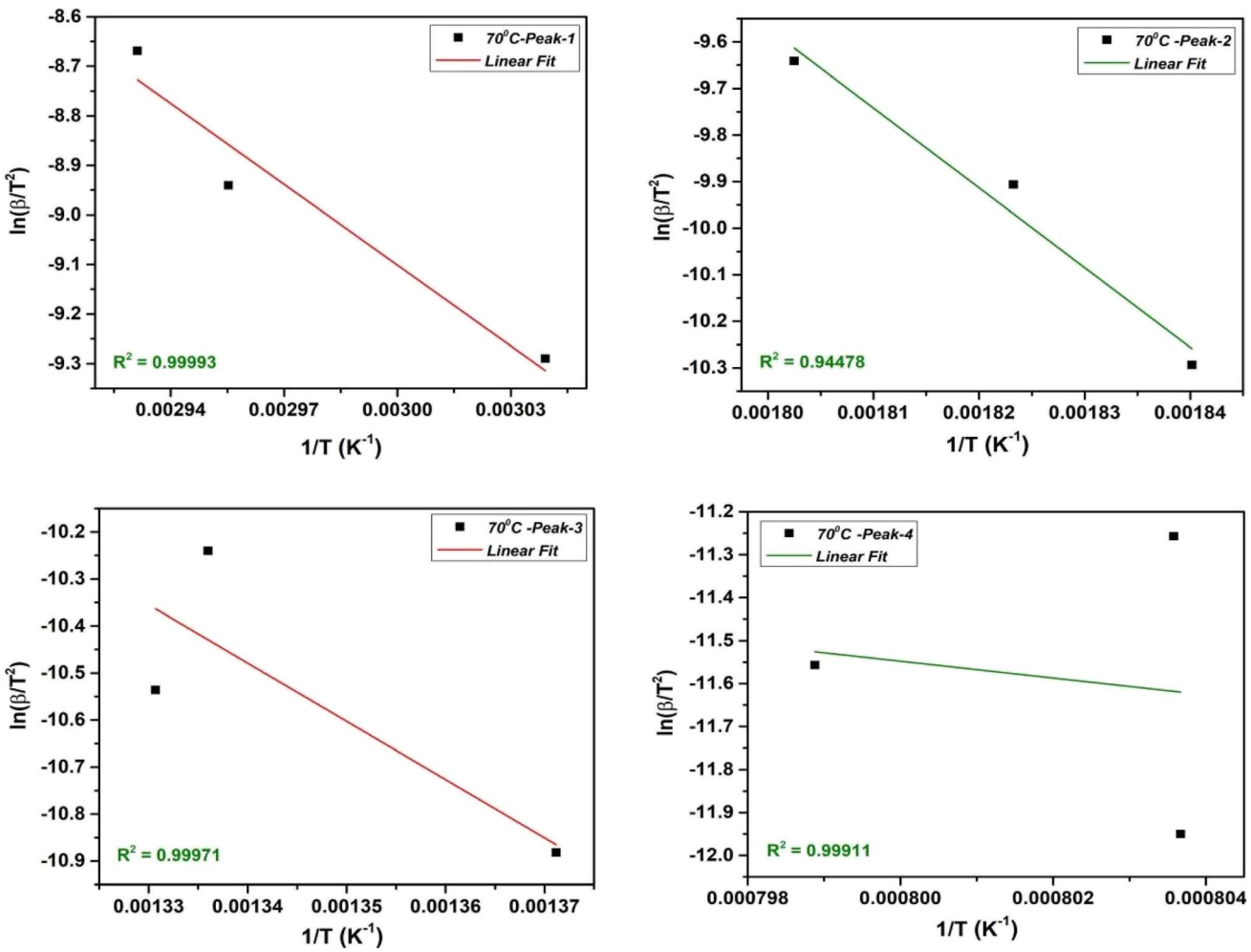

Fig. 6 The KAS plot of four step decomposition for $NbSe_2$ NPs sample synthesized at 70 °C.

© 2024 The Author(s). Published by the Royal Society of Chemistry

Open Access Article. Published on 22 October 2024. Downloaded on 1/27/2026 10:50:57 AM. This article is licensed under a Creative Commons Attribution-NonCommercial 3.0 Unported Licence.

However, for both the non-isothermal and isothermal pyrolysis, the pre-exponential factor is calculated on the assumption of first-order reaction as follows eqn (3),

$$A = \frac{E_a \times \exp(\text{intercept})}{R} \quad (3)$$

2.3.2.2. Flynn–Wall–Ozawa (FWO) method. The FWO method uses the isoconversional approach, which involves analyzing heating rate experiments at a constant conversion level. It calculates E_a as a function of conversion. The FWO method is suitable when the reaction mechanism changes with temperature and provides E_a as a function of conversion. The integral FWO method is based on the eqn (4) as follows;[41,42]

$$\ln \beta = -1.052\left(\frac{E_a}{RT}\right) + \ln\left(\frac{AE_a}{R}\right) - \ln(f(\alpha)) - 5.33 \quad (4)$$

All the variables present in this equation hold similar meanings as discussed in the KAS method. For a constant value of α, a plot of $\ln \beta$ *vs.* $1/T$ has been plotted, which provides a straight line. The slope and intercept allow evaluation of the kinetic parameters as activation energy (E_a), and phonon frequency factor (A),

$$E_a = -\left(\frac{\text{slope} \times R}{1.052}\right) \quad (5)$$

$$A = \frac{R \times \exp(\text{intercept})}{E_a} \quad (6)$$

The FWO plot of the $NbSe_2$ NPs four decomposition steps for samples at R.T., 70 °C, and 100 °C are shown in Fig. 8, 9, and 10 respectively. The peaks are obtained from the differentiation of the thermogravimetric data.

From the value of E_a and A estimated by KAS, and FWO methods. Further kinetic parameters such as a change in ΔH^*, ΔS^*, and ΔG^* are estimated for $NbSe_2$ NPs samples at R.T., 70 °C, and 100 °C using the following equations,[31,43]

$$\Delta H^* = E_a - RT \quad (7)$$

$$\Delta S^* = R \ln\left(\frac{Ah}{k_B T}\right) \quad (8)$$

$$\Delta G^* = \Delta H^* - T\Delta S^* \quad (9)$$

The estimated values of E_a, A, ΔH^*, ΔS^*, and ΔG^* for the $NbSe_2$ NPs samples at R.T., 70 °C, and 100 °C are mentioned in

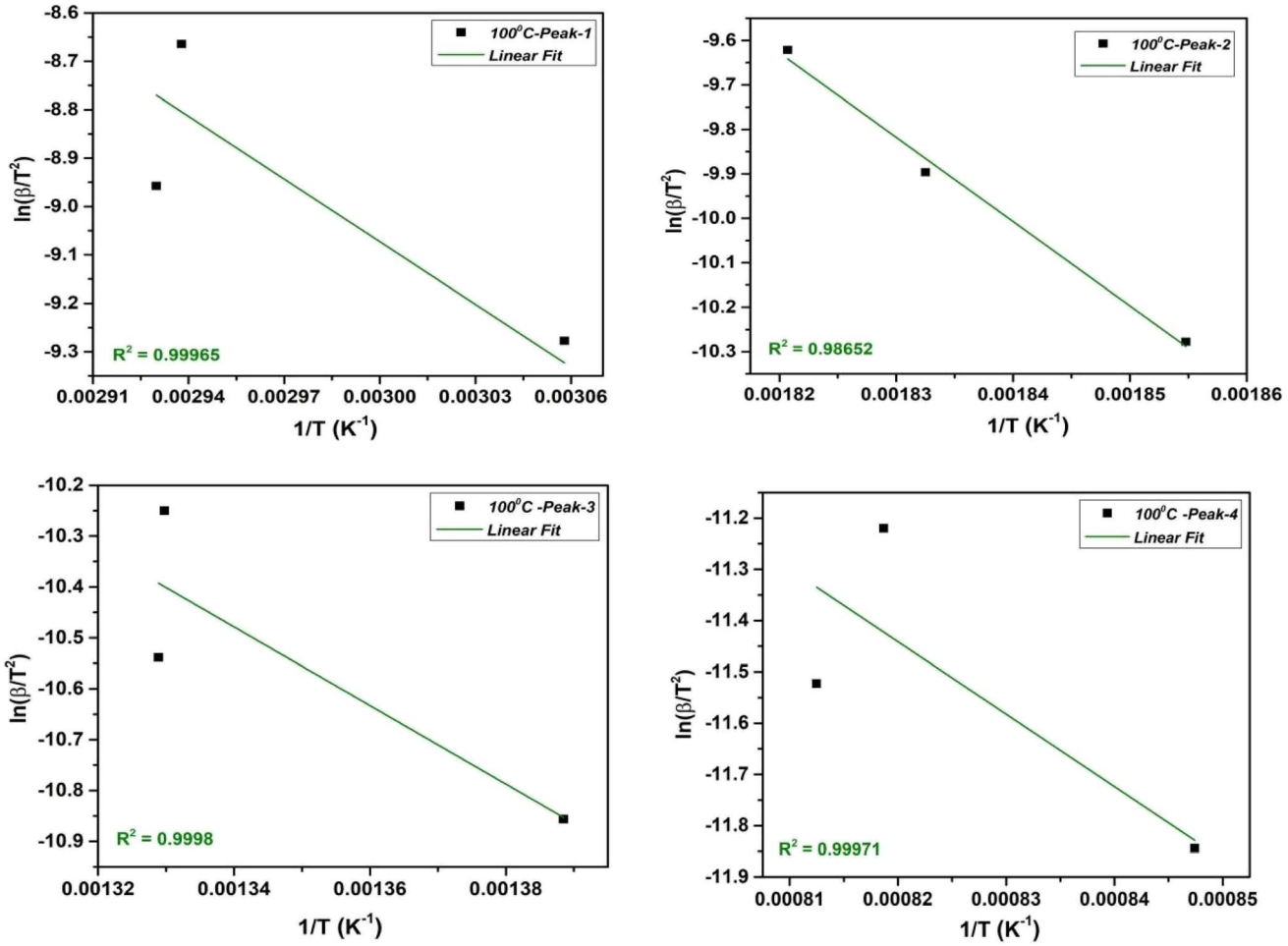

Fig. 7 The KAS plot of four-step decomposition for $NbSe_2$ NPs sample synthesized at 100 °C.

Open Access Article. Published on 22 October 2024. Downloaded on 1/27/2026 10:50:57 AM.
This article is licensed under a Creative Commons Attribution-NonCommercial 3.0 Unported Licence.

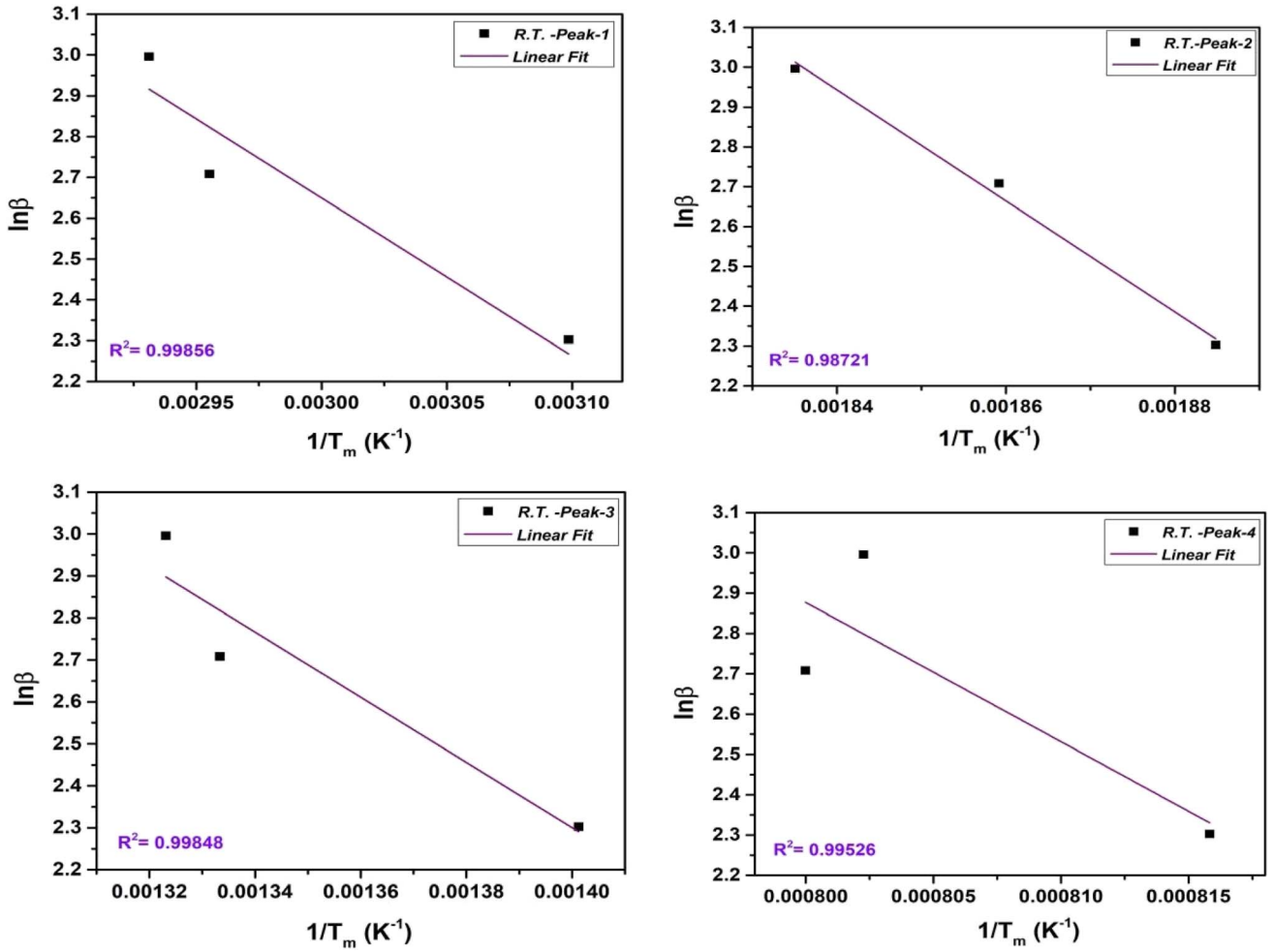

Fig. 8 The FWO plot of four step decomposition for $NbSe_2$ NPs sample synthesized at R.T.

Table 3. The results of different kinetic parameters determined by other methods are near-matched for all samples. This observation confirms the authenticity of the calculations using the above thermal relations.

Based on the data from Table 3, the sample synthesized at 70 °C shows higher activation energies in the first and second steps (45.21 kJ mol^{-1} and 142.39 kJ mol^{-1}, respectively) compared to those at R.T. and 100 °C, indicating that more energy is required for decomposition, which implies greater thermal stability. The pre-exponential factor (A) for the 70 °C sample is significantly higher, particularly when using the FWO method, suggesting a higher frequency of successful collisions leading to the reaction, thereby contributing to improved thermal stability and more uniform reaction kinetics.

Additionally, the sample at 70 °C shows lower ΔH^* values for most steps compared to the 100 °C sample, indicating a reduced energy requirement for decomposition, which is consistent with its enhanced stability at this synthesis temperature. For instance, in the second step, the sample at 70 °C has a ΔH^* of 137.83 kJ mol^{-1} compared to 153.07 kJ mol^{-1} at 100 °C. Moreover, the sample at 70 °C exhibits more negative ΔS^* values, indicating a more ordered transition state compared to R.T. and 100 °C. This is particularly evident in the second step, where the sample at 70 °C has a ΔS^* of -262.12 J K^{-1} mol^{-1} compared to R.T.'s -170.20 J K^{-1} mol^{-1} and the 100 °C sample is -135.84 J K^{-1} mol^{-1}.

Furthermore, the ΔG^* values at 70 °C are generally lower, with the second step showing ΔG^* values of 281.70 kJ mol^{-1} (KAS) and 122.36 kJ mol^{-1} (FWO), lower than those at both R.T. and 100 °C. These findings collectively suggest that the 70 °C sample demonstrates superior thermal stability, making it the optimal temperature for synthesis.

3. Materials and method

3.1. Materials

All the chemicals used were analytical grade. Niobium pentachloride dihydrate ($NbCl_5 \cdot 2H_2O$) [minimum assay 99%, Alfa Assar, United States], hydrochloric acid (HCl) [minimum assay 35%, HiMedia Laboratories Pvt. Ltd, Mumbai, India], triethanol amine (TEA) [minimum assay 98%, Sisco Research Laboratories (SRL) Pvt. Ltd, India], sodium selenite (Na_2SeO_3) [minimum assay 98.5%, HiMedia Laboratories Pvt. Ltd, Mumbai, India] and hydrazine hydrate (N_2H_4) [Sigma-Aldrich Pvt. Ltd, India] are used for the synthesis.

© 2024 The Author(s). Published by the Royal Society of Chemistry

Open Access Article. Published on 22 October 2024. Downloaded on 1/27/2026 10:50:57 AM.
This article is licensed under a Creative Commons Attribution-NonCommercial 3.0 Unported Licence.

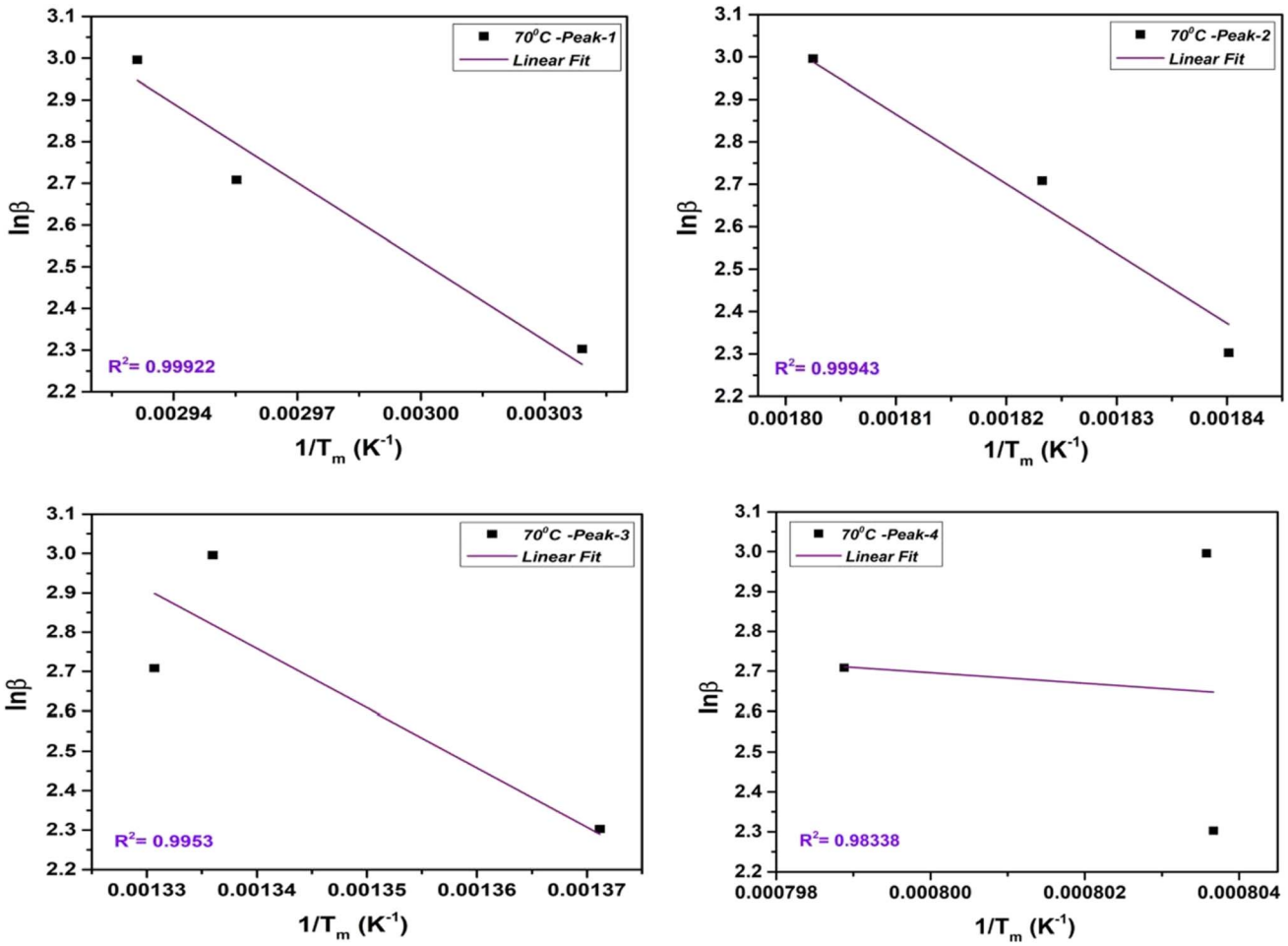

Fig. 9 The FWO plot of four step decomposition for $NbSe_2$ NPs sample synthesized at 70 °C.

3.2. Synthesis of $NbSe_2$ nanoparticles

The synthesis details of $NbSe_2$ NPs utilizing precursor solutions of niobium (Nb) and selenium (Se) at R.T. *via* the sonochemical method are reported earlier.[14] From considering synthesis parameters this synthesis of $NbSe_2$ NPs at R.T., 70 °C and 100 °C, initially, solutions containing Nb and Se precursors were prepared separately. Specifically, niobium chloride pentahydrate ($NbCl_5 \cdot 2H_2O$) was utilized as the source of Nb^+, while sodium selenite (Na_2SeO_3) served as the Se^- source. Additionally, TEA and hydrazine hydrate were introduced as complexing and reducing agents in precursor solution respectively. These precursor solutions were then subjected to ultrasonic waves under continuous stirring. The ultrasonic treatment facilitated the efficient mixing and reaction of the precursors, promoting nucleation and growth of $NbSe_2$ NPs. After the filtration, synthesized nanoparticles dry at the synthesized temperature. Fig. 11 shows the schematic illustration of the synthesis process of $NbSe_2$ nanoparticles synthesized at R.T., 70 °C, and 100 °C *via* the sonochemical method. The synthesized nanoparticles show that at R.T., the sample exhibits a brown color, which remains consistent up to 70 °C. However, above 70 °C, the color begins to change from light black to dark black, becoming more pronounced as the temperature increases, reaching up to 100 °C. These subsequent syntheses allowed for comparative analysis of the resulting NPs synthesized under different temperature conditions, enabling insights into the temperature-dependent effects on nanoparticle morphology, size, crystallinity, and thermal properties.

3.3. Characterizations

The compositional analysis of synthesized nanoparticles was characterized using energy dispersive X-ray analysis with the ultra-high brightness Schottky emitter field emission gun with the energy of 0.0 to 20.0 keV attached with high-resolution Nova Nano SEM-450, FEI, Ltd scanning electron microscope (SICART, Vallabh Vidyanagar). The structural analysis of synthesized nanoparticles was identified through the Bruker D8 Advance X-ray diffraction technique with CuKα radiation in the 2θ range of 1° to 80° (SICART, Vallabh Vidyanagar). Here the thermocurves were recorded by Seiko SII-EXSTAR TG/DTA-7200 at three different heating rates of 10 K (min^{-1}), 15 K (min^{-1}), and 20 K (min^{-1}) under an inert N_2 atmosphere over the temperature gradually ramped up from R.T. (300 K) to a specified maximum temperature up to 1260 K in the case of all samples.

Open Access Article. Published on 22 October 2024. Downloaded on 1/27/2026 10:50:57 AM.
This article is licensed under a Creative Commons Attribution-NonCommercial 3.0 Unported Licence.

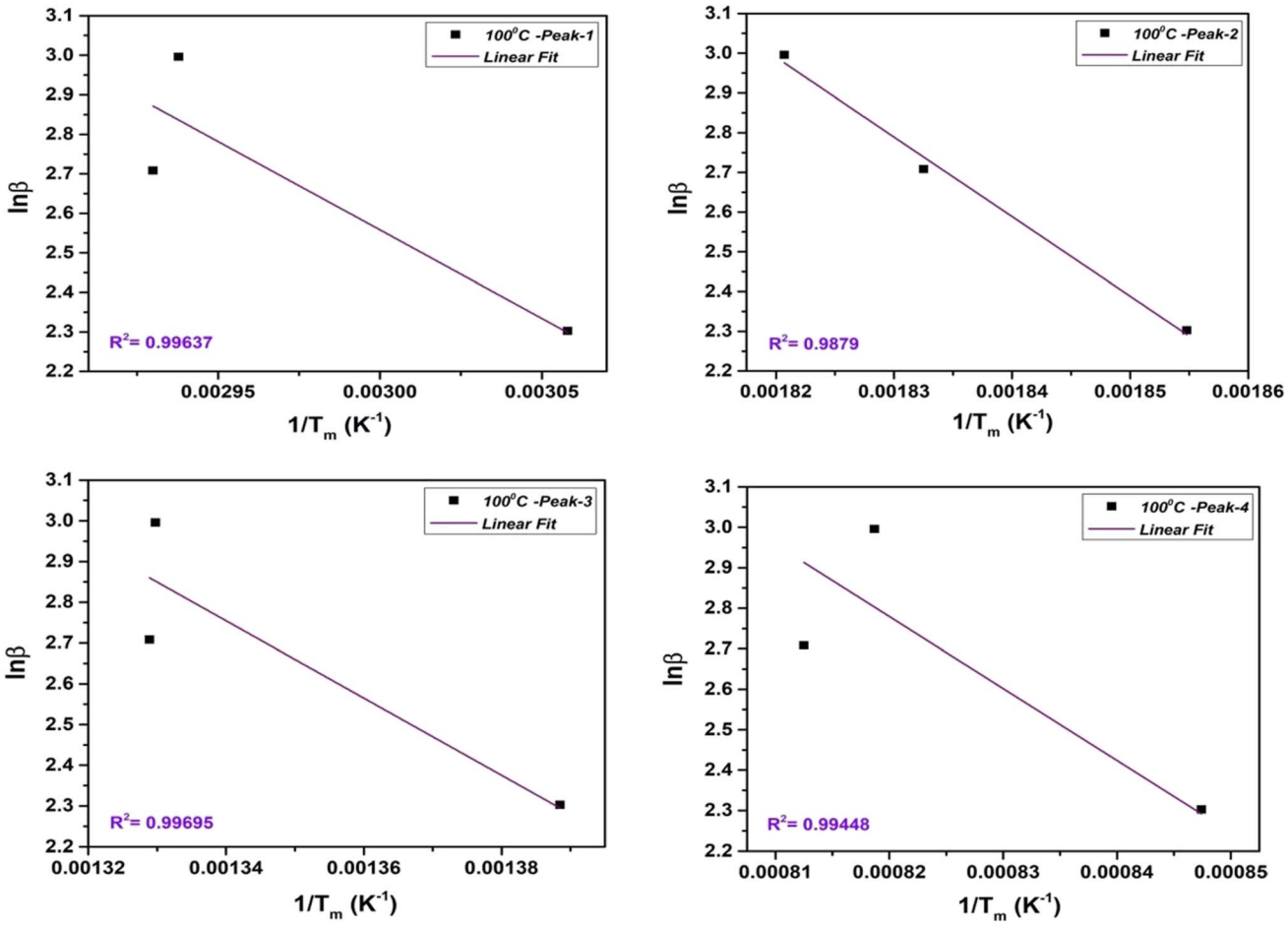

Fig. 10 The FWO plot of four-step decomposition for $NbSe_2$ NPs sample synthesized at 100 °C.

Table 3 The obtained kinetic parameter of $NbSe_2$ NPs synthesized at R.T., 70 °C, and 100 °C

Sample	DTG step	Method	E_a (kJ mol^{-1})	A (S^{-1})	ΔH^* (kJ mol^{-1})	ΔS^* (J K^{-1} mol^{-1})	ΔG^* (kJ mol^{-1})
R.T.	1st	KAS	25.16	$3.39 \times 10^{\circ}$	22.38	−82.55	50.13
		FWO	30.62	5.80×10^{6}	27.84	−58.94	47.53
	2nd	KAS	107.00	1.44×10^{1}	102.53	−170.20	194.06
		FWO	110.21	2.09×10^{7}	105.74	−52.25	123.20
	3rd	KAS	57.24	$7.70 \times 10^{\circ}$	51.09	−178.05	182.81
		FWO	61.35	1.16×10^{7}	55.20	−59.80	75.18
	4th	KAS	303.74	4.09×10^{1}	293.43	−168.47	502.45
		FWO	272.78	5.17×10^{7}	262.46	−51.66	279.72
70 °C	1st	KAS	45.21	7.36×10^{3}	42.41	−114.44	80.89
		FWO	49.83	1.20×10^{10}	47.03	4.46	45.54
	2nd	KAS	142.39	2.32×10^{4}	137.83	−262.12	281.70
		FWO	129.74	3.13×10^{10}	125.18	8.38	122.36
	3rd	KAS	103.02	1.68×10^{4}	96.84	−114.18	181.69
		FWO	118.90	2.87×10^{10}	112.72	5.12	111.00
	4th	KAS	163.09	2.65×10^{4}	152.72	−114.68	295.70
		FWO	105.20	2.54×10^{10}	94.84	−0.179	94.90
100 °C	1st	KAS	35.89	2.07×10^{2}	33.09	−144.13	81.56
		FWO	35.39	3.75×10^{7}	32.60	−43.48	47.22
	2nd	KAS	157.60	9.09×10^{2}	153.07	−135.84	227.06
		FWO	158.41	1.68×10^{8}	153.88	−35.02	172.95
	3rd	KAS	64.22	3.70×10^{2}	58.05	−145.88	166.23
		FWO	74.95	7.93×10^{7}	68.79	−43.82	101.28
	4th	KAS	117.54	6.78×10^{2}	107.47	−144.91	282.82
		FWO	140.57	1.49×10^{8}	130.51	−42.61	182.07

© 2024 The Author(s). Published by the Royal Society of Chemistry

Open Access Article. Published on 22 October 2024. Downloaded on 1/27/2026 10:50:57 AM. This article is licensed under a Creative Commons Attribution-NonCommercial 3.0 Unported Licence.

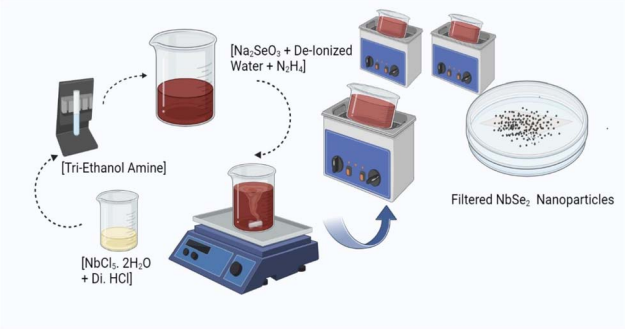

Fig. 11 Shows the schematic illustration of the synthesis of $NbSe_2$ nanoparticles synthesized at R.T., 70 °C, and 100 °C *via* the sonochemical method.

4. Conclusion

In conclusion, the temperature-dependent sonochemical synthesis and subsequent thermal analysis of $NbSe_2$ nanoparticles were studied, revealing significant impacts on their thermal stability, composition, and structural properties. XRD analysis confirmed that the synthesized nanoparticles belong to the $P6_3/mmc$ space group with a hexagonal structure and standard lattice constants $a = b = 3.44$ Å and $c = 12.56$ Å. Among the samples, $NbSe_2$ nanoparticles synthesized at 70 °C exhibited superior characteristics, including the crystallite size (15.12 nm), lowest dislocation density (4.74×10^{-3}), and minimal internal strain (0.43). These properties suggest better crystallinity and fewer defects compared to samples synthesized at R.T. and 100 °C. From the TG, improved thermal properties of 70 °C were attributed to better crystallinity, fewer structural defects, and a composition closer to the desired stoichiometry, as confirmed by EDAX and XRD analysis. From the TG analysis, the sample synthesized at 70 °C had less weight loss% of 70.07, 69.59, and 66.57 at three different heating rates of 10, 15, and 20 K (min^{-1}) compared to that synthesized at R.T. and 100 °C. From TG the observed kinetic parameter sample 70 °C also showed higher activation energies and lower enthalpy change, indicating superior thermal stability. The higher pre-exponential factors and more negative entropy changes for 70 °C suggest more uniform reaction kinetics and a more ordered transition state. These findings underscore the importance of synthesis temperature in tailoring the properties of $NbSe_2$ nanoparticles. The study demonstrates that 70 °C is the optimal temperature for achieving high thermal stability and desired structural characteristics, making these nanoparticles suitable for potential applications in optoelectronic, energy storage, electronics, and catalysis. Future studies should explore the synthesis of $NbSe_2$ nanoparticles at additional intermediate temperatures and under different sonochemical conditions to further refine the understanding of the relationship between synthesis parameters and nanoparticle properties. The limitation of this study is that the material remains thermally stable up to 600 K. The maximum weight loss occurs in the temperature range of 600 to 1200 K. This research provides valuable insights into the temperature-dependent synthesis and thermal behavior of $NbSe_2$ nanoparticles, highlighting their potential in various advanced technological fields.

Data availability

The datasets generated/analyzed during the current study are presented in the article.

Author contributions

SRB contributed to the material preparation, data collection, analysis, and writing of the original draft. MSD acquired resources and assisted in project administration, reviewing, and editing of the manuscript, and supervision. SHC participated in the conceptualization, investigation, and review of the manuscript. TAL participated in the conceptualization, investigation, data analysis, and review.

Conflicts of interest

There are no conflicts to disclose.

Acknowledgements

The work was supported by the Education Department, Govt. of Gujarat, India for providing a research fellowship under SHODH (ScHeme of Developing High-quality Research) (reference no. 202010820001). The authors are very thankful to Dr A. Mahesh, Assistant Professor, C. L. Patel Institute of Studies and Research in Renewable Energy, Charutar Vidya Mandal University for providing lab facilities to conduct the experimental work.

References

1 N. R. Hemanth, T. Kim, B. Kim, A. H. Jadhav, K. Lee and N. K. Chaudhari, *Mater. Chem. Front.*, 2021, **5**, 3298–3321.
2 Q. Fu, J. Han, X. Wang, P. Xu, T. Yao, J. Zhong, W. Zhong, S. Liu, T. Gao, Z. Zhang, L. Xu and B. Song, *Adv. Mater.*, 2021, **33**, 1–24.
3 R. Lv, J. A. Robinson, R. E. Schaak, D. Sun, Y. Sun, T. E. Mallouk and M. Terrones, *Acc. Chem. Res.*, 2015, **48**, 56–64.
4 N. Choudhary, M. A. Islam, J. H. Kim, T. J. Ko, A. Schropp, L. Hurtado, D. Weitzman, L. Zhai and Y. Jung, *Nano Today*, 2018, **19**, 16–40.
5 T. Limbani and A. Mahesh, *Nano-Struct. Nano-Objects*, 2023, **35**, 101010.
6 C. S. Oglesby, E. Bucher, C. Kloc and H. Hohl, *J. Cryst. Growth*, 1994, **137**, 289–294.
7 F. Bischoff, W. Auwärter, J. V. Barth, A. Schiffrin, M. Fuhrer and B. Weber, *Chem. Mater.*, 2017, **29**, 9907–9914.
8 R. Contreras, D. Celentano, T. Luo, Z. Liu and J. O. Morales-Ferreiro, *Nanomaterials*, 2023, **13**, 1–9.
9 N. M. Toporova, E. M. Sherokalova, N. V. Selezneva, V. V. Ogloblichev and N. V. Baranov, *J. Alloys Compd.*, 2020, **848**, 156534.

© 2024 The Author(s). Published by the Royal Society of Chemistry

Open Access Article. Published on 22 October 2024. Downloaded on 1/27/2026 10:50:57 AM. This article is licensed under a Creative Commons Attribution-NonCommercial 3.0 Unported Licence.

10 J. Guo, Y. Shi, C. Zhu, L. Wang, N. Wang and T. Ma, *J. Mater. Chem. A*, 2013, **1**, 11874–11879.
11 C. Su, H. Yan, H. Li, J. Yan, L. Tong, X. Wang, W. Fan, Q. Wang and S. Yin, *J. Colloid Interface Sci.*, 2024, **670**, 28–40.
12 H.-H. Lien, *eCommons*, 2017.
13 C. Wu, J. Liu, B. Liu, S. He, G. Dai, B. Xu and W. Zhong, *J. Mater. Chem. B*, 2019, **7**, 3134–3142.
14 T. Takahashi, C. Ando, M. Saito, Y. Miyata, Y. Nakanishi, J. Pu and T. Takenobu, *npj 2D Mater. Appl.*, 2021, **5**, 1–8.
15 R. He, J. Van Baren, J. A. Yan, X. Xi, Z. Ye, G. Ye, I. H. Lu, S. M. Leong and C. H. Lui, *2D Mater.*, 2016, **3**, 1–7.
16 P. Sekar, E. C. Greyson, J. E. Barton and T. W. Odom, *J. Am. Chem. Soc.*, 2005, **127**, 2054–2055.
17 K. Iwaya, T. Hanaguri, A. Koizumi, K. Takaki, A. Maeda and K. Kitazawa, *Phys. B*, 2003, **329–333**, 1598–1599.
18 Z. Miao, D. Huang, Y. Wang, W. J. Li, L. Fan, J. Wang, Y. Ma, Q. Zhao and Z. Zha, *Adv. Funct. Mater.*, 2020, **30**, 1–13.
19 T. Kolokoto, V. Mashindi, R. Kadzutu-Sithole, L. F. E. Machogo-Phao, Z. B. Ndala, N. P. Shumbula, S. S. Nkabinde, G. N. Ngubeni, S. S. Gqoba, K. P. Mubiayi and N. Moloto, *RSC Adv.*, 2021, **11**, 31159–31173.
20 S. R. Bharucha, M. S. Dave, R. K. Giri, S. H. Chaki and T. A. Limbani, *Adv. Nat. Sci.: Nanosci. Nanotechnol.*, 2024, **15**, 1–9.
21 A. K. Worku, D. W. Ayele, N. G. Habtu, G. A. Melas, T. A. Yemata, N. Y. Mekonnen and M. A. Teshager, *SN Appl. Sci.*, 2021, **3**, 699.
22 M. Naffakh, *Polymers*, 2021, **13**, 1–18.
23 H. Zhang, A. Rousuli, K. Zhang, L. Luo, C. Guo, X. Cong, Z. Lin, C. Bao, H. Zhang, S. Xu, R. Feng, S. Shen, K. Zhao, W. Yao, Y. Wu, S. Ji, X. Chen, P. Tan, Q.-K. Xue, Y. Xu, W. Duan, P. Yu and S. Zhou, *Nat. Phys.*, 2022, **18**, 1425–1430.
24 M. M. Ugeda, A. J. Bradley, Y. Zhang, S. Onishi, Y. Chen, W. Ruan, C. Ojeda-Aristizabal, H. Ryu, M. T. Edmonds, H. Z. Tsai, A. Riss, S. K. Mo, D. Lee, A. Zettl, Z. Hussain, Z. X. Shen and M. F. Crommie, *Nat. Phys.*, 2016, **12**, 92–97.
25 A. Gedanken, *Ultrason. Sonochem.*, 2004, **11**, 47–55.
26 H. Xu, B. W. Zeiger and K. S. Suslick, *Chem. Soc. Rev.*, 2013, **42**, 2555–2567.
27 D. Ghanbari, M. Salavati-Niasari and M. Ghasemi-Kooch, *J. Ind. Eng. Chem.*, 2014, **20**, 3970–3974.
28 J. Zhu, Y. Koltypin and A. Gedanken, *Chem. Mater.*, 2000, **12**, 73–78.
29 S. R. Bharucha, M. S. Dave, R. K. Giri, S. H. Chaki and T. A. Limbani, *Eng. Proc.*, 2023, **56**, 1–7.
30 M. Koraiem Handawy, A. Yu Snegirev, V. V. Stepanov and V. A. Talalov, *IOP Conf. Ser.: Mater. Sci. Eng.*, 2021, **1100**, 012053.
31 S. H. Chaki, M. D. Chaudhary and M. P. Deshpande, *J. Therm. Anal. Calorim.*, 2015, **120**, 1261–1272.
32 M. Heydari, M. Rahman and R. Gupta, *Int. J. Chem. Eng.*, 2015, **2015**, 1–9.
33 N. Kongkaew, W. Pruksakit and S. Patumsawad, *Energy Procedia*, 2015, **79**, 663–670.
34 M. A. Ibrahem, W. C. Huang, T. W. Lan, K. M. Boopathi, Y. C. Hsiao, C. H. Chen, W. Budiawan, Y. Y. Chen, C. S. Chang, L. J. Li, C. H. Tsai and C. W. Chu, *J. Mater. Chem. A*, 2014, **2**, 11382–11390.
35 N. D. Boscher, C. J. Carmalt and I. P. Parkin, *Eur. J. Inorg. Chem.*, 2006, 1255–1259.
36 J. Gao, S. Cheng, X. Zeng, X. Sun, Y. Bai, S. Hu, J. Yue, X. Yu, M. Zhang, X. Xu and M. Han, *Ultrason. Sonochem.*, 2024, **108**, 106978.
37 I. Milosavljevic and E. M. Suuberg, *Ind. Eng. Chem. Res.*, 1995, **34**, 1081–1091.
38 A. J. Khimani, S. H. Chaki, R. K. Giri, R. R. Meena, R. M. Kannaujiya and M. P. Deshpande, *Chem. Thermodyn. Therm. Anal.*, 2023, **9**, 100104.
39 A. W. Coats and J. P. Redfern, *Natu. Pub. Gr.*, 1964, **201**, 68–69.
40 H. E. Kissinger, *Anal. Chem.*, 1957, **29**, 1702–1706.
41 T. Ozawa, *Thermochim. Acta*, 1992, **203**, 159–165.
42 T. J. Malek, S. H. Chaki, J. P. Tailor and M. P. Deshpande, *AIP Conf. Proc.*, 2016, 020390.
43 S. H. Chaki, *Front. Mater. Sci. China*, 2008, **2**, 322–325.

© 2024 The Author(s). Published by the Royal Society of Chemistry